

The Nature of Associated Absorption and the UV–X-ray Connection in 3C 288.1

Frederick W. Hamann

Department of Astronomy, University of Florida, 211 Bryant Space Sciences Center, Gainesville, FL 32611-2055 (*hamann@astro.ufl.edu*)

Hagai Netzer

Tel Aviv University, School of Physics and Astronomy, Tel Aviv, 69978 Israel

and

Joseph C. Shields

Department of Physics and Astronomy, Clippinger Research Labs 251B, Ohio University, Athens, OH 45701-2979

ABSTRACT

We discuss new *Hubble Space Telescope* spectroscopy of the radio-loud quasar, 3C 288.1. The data cover \sim 590 Å to \sim 1610 Å in the quasar rest frame. They reveal a wealth of associated absorption lines (AALs) with no accompanying Lyman-limit absorption. The metallic AALs range in ionization from C III and N III to Ne VIII and Mg X. We use these data and photoionization models to derive the following properties of the AAL gas: 1) There are multiple ionization zones within the AAL region, spanning a factor of at least \sim 50 in ionization parameter. 2) The overall ionization is consistent with the “warm” X-ray continuum absorbers measured in Seyfert 1 nuclei and other QSOs. However, 3) the column densities implied by the AALs in 3C 288.1 are too low to produce significant bound-free absorption at any UV–X-ray wavelengths. Substantial X-ray absorption would require yet another zone, having a much higher ionization or a much lower velocity dispersion than the main AAL region. 4) The total hydrogen column density in the AAL gas is $\log N_{\text{H}}(\text{cm}^{-2}) \approx 20.2$. 5) The metallicity is roughly half solar. 6) The AALs have deconvolved widths of \sim 900 km s $^{-1}$ and their centroids are consistent with no shift from the quasar systemic velocity (conservatively within \pm 1000 km s $^{-1}$). 7) There are no direct indicators of the absorber’s location in our data, but the high ionization and high metallicity both suggest a close physical relationship to the quasar/host galaxy environment.

Finally, the UV continuum shape gives no indication of a “blue bump” at higher energies. There is a distinct break of unknown origin at \sim 1030 Å, and the decline toward higher energies (with spectral index $\alpha \approx -1.73$, for $f_{\nu} \propto \nu^{\alpha}$) is even steeper than a single power-law interpolation from 1030 Å to soft X-rays.

Subject headings: Galaxies: active; Quasars: absorption lines; Quasars: general; Quasars: individual (3C 288.1)

1. Introduction

Associated absorption lines (AALs) in quasar spectra provide unique information on the kinematics, physical conditions and elemental abundances in the gas near quasars. AALs are defined empirically as having 1) relatively narrow profiles (less than a few hundred km s^{-1}), and 2) absorption redshifts, z_a , near the emission redshift, z_e , (generally within 3000–5000 km s^{-1} , see Weymann et al. 1979, Foltz et al. 1986, Foltz et al. 1988). The first criterion distinguishes AALs from the class of broad absorption lines (BALs), which have velocity widths and maximum displacements that often exceed 10,000 km s^{-1} . BALs clearly form in high-velocity winds from the central engines (see the reviews by Weymann 1997, Weymann 1995, Turnshek 1995, Weymann et al. 1985). AALs (or $z_a \approx z_e$ systems) can form potentially in a variety of locations — from outflows near the black hole/accretion disk, perhaps like the BALs, to intervening gas or galaxies at large (cosmologically significant) distances. A few AAL systems are known to form in quasar ejecta (probably within a few pc of the energy source, Hamann et al. 1997, Barlow & Sargent 1997, Ganguly et al. 1999), while others clearly probe extended regions on host-galaxy scales (>1 kpc distant, Williams et al. 1975, Sargent et al. 1982, Morris et al. 1986, Tripp et al. 1996, Barlow et al. 1997). Surprisingly little else is known about the nature of the absorbing regions or their relationship to other quasar phenomena.

One important clue is that both AALs and BALs in the UV appear to correlate with the presence of continuous absorption in soft X-rays (Green & Mathur 1996, Crenshaw et al. 1999, Mathur et al. 1998, Mathur et al. 1999, Gallagher et al. 1999, Brandt et al. 1999 and references therein). The X-ray absorbers in AAL sources (both quasars and Seyfert 1 galaxies) tend to have high total hydrogen column densities ($\log N_{\text{H}}(\text{cm}^{-2}) \sim 21$ to 23) and high ionizations (being dominated by absorption edges of O VII and O VIII near 0.8 keV) (Reynolds 1997, George et al. 1998a). In contrast, the AALs typically indicate lower column densities and lower levels of ionization (cf. Hamann 1997). The X-ray absorbers that accompany BALs have even larger total column densities of $\log N_{\text{H}}(\text{cm}^{-2}) \gtrsim 23$ (Green & Mathur 1996, Gallagher et al. 1999). In those objects, the total column densities derived from X-rays exceed prior estimates from the BALs by 2 or more orders of magnitude (Hamann 1998). Clearly, we must consider the UV and X-ray data together to obtain a complete census and understanding of the absorbing environments.

A key question now is the physical relationship between the UV and X-ray absorbers. Mathur et al. (1998 and refs. therein) argue that they could reasonably identify a single absorbing medium, while other work has shown that multiple regions (having different velocities, ionizations and/or column densities) are at least sometimes present (e.g. Kriss et al. 1996, Hamann et al. 1997, Reynolds 1997, George et al. 1998b, Mathur et al. 1999). High-ionization UV lines, such as Ne VIII $\lambda\lambda 770,780$ and Mg X $\lambda\lambda 610,625$, can directly test the UV–X-ray relationship because their ionization requirements are similar to the O VII and O VIII edges measured in X-rays. The far-UV spectra needed to reach the Ne VIII and Mg X lines also encompass many under-utilized diagnostics such as the H I Lyman limit, the Lyman series lines, and numerous metal lines spanning a wide range of ionizations. Unfortunately, these features are difficult or impossible to measure in many sources because of their short wavelengths. For example, they are obscured by Galactic Lyman-limit absorption in low-redshift sources (e.g. in all Seyfert galaxies) and contaminated by the dense “forest” of Ly α absorbers at high redshifts. Another problem at

high redshifts is that the dominant O VII and O VIII edges are shifted out of the sensitive energy range of current X-ray telescopes.

Intermediate-redshift quasars ($0.5 \lesssim z \lesssim 1$) provide a unique opportunity to measure all of the key UV and X-ray features in the same object. We have begun a program to obtain UV and X-ray spectra of several such objects. Here we discuss new UV observations of the radio-loud quasar, 3C 288.1. This source has both the required moderate redshift, $z_e \approx 0.961$ (Schmidt 1968), and a strong AAL system (Wills et al. 1995). It also has a dramatically bipolar (lobe-dominated) radio morphology (Reid et al. 1995, Akujor et al. 1994). The X-ray absorption properties of 3C 288.1 are not yet known, but it was weakly detected in soft X-rays with the *Einstein* IPC (from ~ 0.16 to ~ 3.5 keV, Zamorani et al. 1981). Wilkes et al. (1994) estimate its 2-point power-law index between 2500 Å and 2 keV to be $\alpha_{ox} = -1.51$ (where $f_\nu \propto \nu^{\alpha_{ox}}$).

2. Observations and Data Reductions

We obtained spectra of 3C 288.1 in two observations with the *Hubble Space Telescope* (*HST*). Both measurements used the Space Telescope Imaging Spectrograph (STIS) with a $0.2'' \times 52''$ slit and the MAMA detectors. The first observation, on 12 January 1999, yielded 8564 s of on-source integration time in 3 exposures with the G230L grating. The usable wavelength coverage is ~ 1645 Å to ~ 3160 Å (observer's frame). The realized spectral resolution depends mostly on the line-spread function of the spectrograph for the quasar point source. We measure this resolution to be roughly 5.9 Å, or 3.7 pixels on the MAMA detector, based on the full widths at half minimum (FWHMs) of Galactic absorption lines. The velocity resolution is thus ~ 1080 to ~ 560 km s $^{-1}$ from the short- to long-wavelength ends of the spectral coverage. The second observation, on 21 January 1999, used the G140L grating for a total of 14778 s in 5 exposures. The spectral coverage in this case is roughly 1155 to 1720 Å at a measured resolution of ~ 2.5 Å (~ 4.2 pixels on the MAMA), corresponding to ~ 660 to ~ 440 km s $^{-1}$ from the short- to long-wavelength ends. The combined spectra provide complete wavelength coverage from ~ 590 Å to ~ 1610 Å in the quasar rest frame.

We acquired flux-calibrated spectra for these observations (one spectrum for each exposure) from the Space Telescope Science Institute, based on their standard “pipeline” reductions. We then performed additional manipulations and measurements using the IRAF¹ software package. In particular, we measured Galactic absorption lines to establish that there are no significant wavelength shifts between exposures taken with the same grating. We then averaged the 3 G230L spectra and the 5 G140L spectra using weights determined from the integration times. To check the absolute wavelength calibrations with each grating, we measured centroids for several Galactic absorption lines in the two averages. Based on those measurements, and assuming the Galactic lines are at their laboratory wavelengths (Schneider et al. 1993), we applied offsets of -1.25 Å and -0.2 Å to the mean G230L and G140L spectra, respectively.

¹IRAF is distributed by the National Optical Astronomy Observatories, which operates under the Association of Universities for Research in Astronomy in cooperative agreement with the National Science Foundation.

3. Results

Figure 1 shows the final mean spectra. They reveal many new AALs compared to earlier work (Wills et al. 1995), including Ne VIII $\lambda\lambda 770,780$ and probably Mg X $\lambda 625$. They also show no H I Lyman limit absorption related to the AALs (see also Fig. 3 below).

3.1. Absorption Lines

Table 1 lists properties of the detected absorption lines, namely, the vacuum centroid wavelengths (λ_{obs}) and equivalent widths (W_λ) in the observed frame (both in Å), the line identifications (ID), the absorption redshifts (z_a) for identified non-Galactic features, and the derived column densities as discussed in §4.2 below. The derived quantities use laboratory wavelengths and atomic data from Verner et al. (1994a). The strong AAL system has a nominal redshift of $z_a \approx 0.9627$. Table 1 includes upper limits on W_λ for several lines *not* detected in this system. The last column in the table provides additional notes, including FWHMs for the strongest unblended lines at $z_a \approx 0.9627$.

We measure the absorption lines by first defining a pseudo-continuum based on smooth polynomial fits to the actual continuum and broad emission lines. We then use cursor functions in IRAF’s `splot` program to measure (by direct integration) significant absorption features relative to the fitted curve. For unblended lines, the uncertainties in W_λ are dominated by the subjective pseudo-continuum placement. We estimate the 1σ uncertainties for these features to be $\lesssim 0.1$ Å in the G140L data and $\lesssim 0.15$ Å in G230L. For absorption features blended with each other, the uncertainties depend on the severity of the blend. If the blending is not severe (i.e. if there are still distinct absorption minima at each transition’s wavelength), we again measure/deblend the individual lines “by eye” using cursor functions in `splot`. To check our accuracy, we also fit some of these modestly blended lines with gaussian profiles (using χ^2 minimization in the IRAF task `specfit`). Figure 2 shows a blend of 4 such lines, including Ly β and the O VI doublet in the $z_a \approx 0.9627$ system. We fit these features with one gaussian per transition (see dotted curves in figure). The redshifts and velocity widths of the O VI pair are forced to be identical. The measurements derived from these fits appear in Table 1. They are within 10% of our estimates from manual deblending, thus confirming the viability of both procedures.

Some severe blends in the $z_a \approx 0.9627$ system do not have distinct absorption dips corresponding to each transition. For the multiplets in this category, C IV $\lambda\lambda 1549,1551$, N V $\lambda\lambda 1239,1243$ and N III $\lambda\lambda 685,686$ (Fig. 1), we make no attempt at deblending and list them as single lines in Table 1. For other unresolved blends, we measure W_λ for the entire blend and then divide the result among the different transitions. The W_λ for both the entire blend and the individual lines are given in Table 1. In particular, O V $\lambda 608$ is part of an unresolved blend with Galactic Si II $\lambda\lambda 1190,1193$. We estimate W_λ for O V $\lambda 608$ alone by subtracting a prediction for the Galactic Si II (1.4 Å), based on the relative strengths of the various Si II lines in other quasar spectra (Schneider et al. 1993). The result is given in Table 1 without further correction for the possible contribution from Mg X $\lambda 610$. Another case involves O IV $\lambda 788$ and S V $\lambda 786$, which are blended with each other and with Galactic C IV $\lambda\lambda 1549,1551$ absorption. For this blend, we first subtract a C IV contribution (0.6 Å) derived from the Galactic C IV/Si IV ratio in other sources

(Schneider et al. 1993). We then divide the remaining W_λ between the O IV and S V lines according to the ratio (3.55:1) of their oscillator strengths weighted by solar abundances (i.e. their “strength” parameters in Verner et al. 1994a).

Finally, we note that the measurement uncertainties are particularly large for the Ly α absorption at $z_a \approx 0.9627$ because it lies near a sharp peak in the Ly α emission line (Fig. 1). Our estimate of this Ly α absorption strength is therefore sensitive to the assumed emission profile. In §4.3 we will show that the value of W_λ given for this line in Table 1 is almost certainly too small. The 1σ uncertainties in the O VI, N V and C IV AALs, which also sit atop emission lines, should be $<10\%$ based on repeated measurements with different assumed emission-line profiles.

3.2. Emission Lines

We measure the emission lines using our fit above to the pseudo-continuum (§3.1). This fit (for example Figure 2) interpolates across the absorption features and thus approximates the unabsorbed emission spectrum. We define the line emission relative to a subjective estimate of the “true” continuum in this fitted spectrum. Direct integration then yields approximate rest-frame equivalent widths of $W_\lambda = 21 \pm 2$ Å for C IV $\lambda 1549$, $W_\lambda = 12 \pm 3$ Å for O VI $\lambda 1034$, and $W_\lambda = 50 \pm 5$ Å for the Ly α + N V $\lambda 1240$ blend. The 1σ uncertainties are estimates based on multiple measurements with different plausible continuum placements. We estimate a 3σ upper limit on the Ne VIII $\lambda 774$ equivalent width of very roughly 7 Å, consistent with the measured strength of this feature in other QSOs (Hamann et al. 1998).

3.3. Continuum Shape

Figure 3 shows the combined *HST*-STIS spectra on a log-log scale with frequencies shifted to the quasar rest frame. There is a clear change in the continuum slope near 1030 Å ($\log \nu(\text{Hz}) \approx 15.46$). This change is illustrated in the figure by a broken power-law ($f_\nu \propto \nu^\alpha$) with $\alpha \approx -1.73$ for $\lambda \lesssim 1030$ Å and $\alpha \approx -0.83$ for $\lambda \gtrsim 1030$ Å. A break like this near 1030 Å appears to be typical of QSOs (Zheng et al. 1997, O’Brien et al. 1988), although the spectral indices derived here are less negative (by 0.2–0.7 dex) than the published averages for other radio-loud sources.

It is interesting to compare the UV continuum fluxes in Figures 1 and 3 with the soft X-ray measurements of 3C 288.1 (Wilkes et al. 1994). In particular, the 2-point power-law index between 2 keV and 1030 Å in the rest frame is $\alpha_{uvx} \approx -1.51$. Note that the X-ray measurement is just a $\sim 3\sigma$ detection and that those data were obtained ~ 19.5 years prior to our *HST* observations. Also note that the value of α_{uvx} given here is coincidentally identical to α_{ox} (between 2 keV and 2500 Å) reported by Wills et al. (1994). They used the same X-ray data but a different (ground-based) measurement of the rest-frame UV. Evidently, the UV flux varied. The X-rays might have varied also. Nonetheless, the slope we measure at $\lambda \lesssim 1030$ Å appears, like other radio-loud quasars, to be significantly steeper than a single power-law extrapolation from 1030 Å to soft X-rays (Laor et al. 1997). The implications of this continuum shape are discussed in §5.3 below.

3.4. UV Variability Check

Wills et al. (1995) observed 3C 288.1 with the Faint Object Spectrograph (FOS) on board *HST* in April 1993. Those spectra span observed wavelengths from 2225 to 3280 Å at a resolution slightly higher than our STIS data, $\text{FWHM} \approx 230 \text{ km s}^{-1}$. Direct comparisons between the two data sets reveal no significant changes in the continuum (from 1135 to 1610 Å in the rest frame) or the emission or absorption lines (Ly α , N V and C IV) measured in common.

4. Properties of the Associated $z_a \approx 0.9627$ Absorber

4.1. Kinematics

The line profiles in the $z_a \approx 0.9627$ system are marginally resolved, with typical measured FWHMs of $\sim 1100 \text{ km s}^{-1}$ (Table 1). Simple gaussian deconvolution from the instrumental response profile therefore suggests that the intrinsic line widths are roughly 900 km s $^{-1}$. We cannot rule out the possibility that these widths result from a blend of many narrower (unresolved) features. However, the higher resolution (230 km s $^{-1}$) FOS spectra of Wills et al (1995, see §3.4 above) give no indication of narrower features in Ly α , C IV or N V. The $\sim 900 \text{ km s}^{-1}$ line widths should, in any case, represent the full line-of-sight velocity dispersion through the absorbing region.

We do not have an accurate estimate of the absorber's velocity shift relative to the quasar. The emission redshift quoted in the literature, $z_e \approx 0.961$, comes from an old photographic measurement of C III] $\lambda 1909$ and Mg II $\lambda 2799$ (Schmidt 1968). Nonetheless, the difference between that z_e and our measurement of $z_a \approx 0.9627$ is consistent with the apparent small blueshift of the AALs relative to the emission-line peaks (e.g. in C IV, Ly α , and O VI, Fig. 1). Interpreting this velocity shift, roughly 250 km s $^{-1}$, in terms of a radial flow is problematic, however, because the broad emission lines might be either blue or redshifted with respect to the quasar's true systemic velocity. For example, Marziani et al. (1996) measured velocity shifts up to ± 1000 in C IV relative to the narrow emission lines (e.g. [O III] $\lambda\lambda 4959, 5007$) in a sample of radio-loud quasars. We therefore conclude conservatively that the AALs in 3C 288.1 lie within $\pm 1000 \text{ km s}^{-1}$ of the quasar's systemic velocity.

4.2. Column Densities

We use a curve-of-growth analysis to derive column densities for each of the ions detected at $z_a \approx 0.9627$. With the line equivalent widths from Table 1, the only free parameter in this analysis is the doppler b value (where $b = \text{FWHM}/1.665$ for gaussian line profiles). Even though the line profiles are not well resolved, the data provide several independent constraints on b and the inferred column densities. In particular, 1) the deconvolved FWHMs, roughly 900 km s $^{-1}$ (§4.1), require $b \lesssim 540 \text{ km s}^{-1}$. 2) The absence of an H I absorption edge at 912 Å (see Figs. 1 and 3) places a firm upper limit on the H I column density and thus a lower limit on the Lyman-line b value. We estimate that the optical depth at this edge is no more 10%, implying an H I column of $\log N_{\text{HI}}(\text{cm}^{-2}) < 16.2$

cm^{-2} and $b \gtrsim 190 \text{ km s}^{-1}$ in the Lyman lines. 3) Comparing different lines of the same ion, such as the H I Lyman series and doublets like O VI and Ne VIII, places firm limits on their b values and column densities. The fact that these multiplets do not have observed ratios of $\sim 1:1$ (Fig. 1 and Table 1) implies immediately that the lines are not dominated by very optically thick components (with small b). Finally, 4) weak lines of low-abundance elements like P V $\lambda\lambda 1118, 1128$ are not detected. If the metals have roughly solar relative abundances, the absence of these weak transitions implies that strong transitions like C IV $\lambda 1548$ have optical depths $\lesssim 30$ (Hamann 1998).

Table 1 lists the column densities derived from each measured line in two limiting cases, $b = 200 \text{ km s}^{-1}$ and $b = 540 \text{ km s}^{-1}$. Higher b values would exceed the deconvolved FWHMs, while lower b values would violate the upper limit on $N(\text{H I})$ and yield inconsistent results for some multiplets (e.g. H I and O VI $\lambda\lambda 1032, 1038$). Comparing these two results in Table 1 gives an indication of the theoretical uncertainties. Note that the results for $b = 540 \text{ km s}^{-1}$ are all within 0.2 dex of the optically thin lower limits.

We adopt an intermediate value of $b = 300 \text{ km s}^{-1}$ for our “best guess” column densities. These columns are listed in Table 2 after averaging over all useful lines for each ion. Entries marked “:” are uncertain by as much as a factor of ~ 2 , while those labeled “::” have even larger uncertainties. C III, Mg X and S V have these uncertainty flags because of blending problems, while S III and S IV have large uncertainties because different lines yield substantially different column density results (Table 1). O V is marked as uncertain because the only line measured for that ion, $\lambda 630$, might be saturated. (The curve-of-growth analysis with $b = 300 \text{ km s}^{-1}$ suggests that O V $\lambda 630$ has optical depths up ~ 7 , higher than any other measured line.)

Note that the analysis above assumes the absorber fully covers the background light source(s) along our line(s) of sight. Partial coverage is known to occur in some AAL systems, based on measured doublet ratios in high resolution spectra (Wampler et al. 1993, Petitjean et al. 1994, Hamann et al. 1997, Barlow et al. 1997, Ganguly et al. 1999, also §5.2 below). The only 2 known cases of partial coverage in radio-loud quasars have coverage fractions of $> 95\%$ (Barlow & Sargent 1997, Hamann et al. 1999). The strongest constraint on the coverage fraction in 3C 288.1 comes from the measured depth of the deepest line, O V $\lambda 630$, which requires $> 75\%$ coverage. If the coverage fraction is near 75%, then the column densities listed for the deepest lines in Table 2 could be underestimated. On the other hand, if the coverage fraction is $> 95\%$ like the other radio-loud quasars, all of the column densities in Table 2 would be accurate.

Clearly, the column densities reported here should be checked with higher resolution spectra. Such data would test for both partial coverage and narrow (presently unresolved) line components. Narrow lines (with low b values) might, in principle, harbor large column densities while contributing little to the total equivalent widths. However, the line multiplet ratios and the lack of a Lyman edge already prohibit low b values and large column densities for the *dominant* absorber in 3C 288.1 (even if there is incomplete coverage). The column densities in Table 2 should therefore apply to whatever absorber(s) control the measured equivalent widths. We will adopt these column densities hereafter in our discussion, with the understanding that they apply strictly to the dominant AAL absorber.

4.3. Ionization, Density and Radial Distance

The detected metal lines at $z_a \approx 0.9627$ range in ionization from C III and N III to Ne VIII and Mg X. There are no strong transitions of higher ions, for example Si XII $\lambda\lambda 499,521$, within our wavelength coverage. The upper limit of the ionization is therefore unknown. The lower limit is firmly established by the absence of singly-ionized metals such as C II, N II and O II (see Table 1).

We assume the absorber is in photoionization equilibrium with the quasar radiation field and we use the numerical code CLOUDY (version 90.04, Ferland et al. 1998) to examine its ionization properties. We note that the column densities in Table 2 imply immediately that the absorber is optically thin in the Lyman continuum, out to at least ~ 0.37 keV (the ionization threshold of Mg X). Figure 4 plots calculated ionization fractions for H I and various metal ions, M_i , in general optically thin clouds that are photoionized by a broken power-law spectrum. We use a spectral index of $\alpha = -1.7$ in the Lyman continuum out to 1 keV, based mainly on our measurement of $\alpha = -1.73$ for $\lambda \lesssim 1030$ Å (§3.3). At higher energies we adopt the slope $\alpha_x = -0.9$, based on X-ray observations of similar objects (Laor et al. 1997, George et al. 1998a). There is considerable uncertainty about the true spectral shape of 3C 288.1 (and other quasars) in the extreme UV and soft X-rays. The uncertain slope is particularly important when comparing ions/lines with very different ionization energies. However, these uncertainties are not important to our main conclusions below.

The ion fractions in Figure 4 are plotted for a range of ionization parameters, U — defined here as the dimensionless ratio of hydrogen-ionizing photon to hydrogen particle densities² (see Ferland et al. 1998). The ionization fractions are not sensitive to either the metal abundances or the space density (for a given U). They also do not depend on the column densities used in the calculations, as long as the gas remains optically thin in the ionizing continuum (see Netzer 1996, Hamann et al. 1995, Hamann 1997 for more discussion and calculations using other parameters).

We estimate U in the 3C 288.1 absorber by comparing the ion fractions $f(M_i)$ in Figure 4 to various column density ratios from Table 2. Each column density ratio yields an independent estimate. Some of the U values are illustrated in Figure 4 by bold vertical lines that connect the $f(M_i)$ curves used for that estimate. For example, the measured N III/N IV column density ratio is -0.6 dex, implying a moderate ionization with $\log U \approx -1.7$. The C III/C IV and O III/O IV ratios suggest similar U . (Although included in Figure 4, we consider the U estimates for sulfur to be unreliable because of the uncertainties in their column densities, §4.2.) By making the reasonable assumption that O, Ne and Mg have roughly solar relative abundances, we use the O VI/Ne VIII and Mg X/Ne VIII column densities to infer much larger values of $\log U \approx 0.0$ in the region where those lines form. The ratios of intermediate ions like N IV/N V and O V/O VI indicate intermediate U values³.

²For comparison, we note that $\log U_x = \log U - 1.47$ for this continuum shape, where U_x is the ionization parameter defined over the photon energies 0.1 to 10 keV (Netzer 1996).

³Note that these simple U estimates do not correct for multiple zones possibly contributing to the measured column densities. Such corrections would require an explicit (but ad hoc) model.

The differences in these derived U values are well above the uncertainties and inconsistent with a single zone absorber. For a given space density, n_H , and distance, R , from the ionizing continuum source, optically thin clouds should have the same level of ionization throughout (e.g. there can be no gradient in the ionization due to the absorber's own opacity). The optically thin clouds in 3C 288.1 must therefore occupy a range of densities or distances. From the definition of U (where $U \propto n_H^{-1} R^{-2}$), and the difference of $\Delta \log U \gtrsim 1.7$ between the “high” and “low”-ionization regions, we infer a factor of $\gtrsim 50$ range in the space density, a factor of $\gtrsim 7$ range in the distance, or some equivalent combination of different n_H and R values.

4.4. Elemental Abundances

The relative abundance of any two elements a and b can be derived from the following expression,

$$\left[\frac{a}{b} \right] = \log \left(\frac{N(a_i)}{N(b_j)} \right) + \log \left(\frac{f(b_j)}{f(a_i)} \right) + \log \left(\frac{b}{a} \right)_\odot \quad (1)$$

where $(b/a)_\odot$ is the solar abundance ratio (Grevesse & Anders 1989), and N and f are respectively the column densities and ionization fractions of element a in ion state i , etc. With suitable ionization corrections, $f(b_j)/f(a_i)$ from Figure 4, we can trivially derive abundance ratios from the column densities in Table 2. For example, we estimate average values of $[\text{C}/\text{O}] \approx -0.5$ and $[\text{N}/\text{O}] \approx +0.1$ from the ratios $\text{C III}/\text{O III}$, $\text{C IV}/\text{O IV}$, $\text{N III}/\text{O III}$ and $\text{N IV}/\text{O IV}$. The theoretical uncertainties in these results (e.g. for different continuum shapes) should be small, $\lesssim 0.1$ dex (at 1σ or $\sim 60\%$ confidence), because we are comparing similar ions (Hamann 1997). The observational uncertainties are larger but more difficult to assess; we estimate that they are < 0.2 dex in these averaged ratios (§4.2 and Table 2). We derive the overall metallicity by assuming the H I absorber resides mainly with the doubly- and triply-ionized metals at $\log U \approx -1.8$ to -1.6 (Fig. 4, §4.3). Plugging the appropriate ion fractions into Equation 1 then implies $[\text{C}/\text{H}] \approx -0.7$, $[\text{N}/\text{H}] \approx -0.1$, and $[\text{O}/\text{H}] \approx -0.3$. The theoretical uncertainties in this case are larger, perhaps up to 0.3–0.4 dex (Hamann 1997), because the ions being compared have significantly different ionization energies.

If we had assumed that most of the H I coexists with the high ions at $\log U \approx 0.0$ (Fig. 4, §4.3), we would have inferred much lower metallicities of $[\text{M}/\text{H}] \approx -1.7$ to -1.4 for the metals O, Ne and Mg. However, these low metallicities would lead to a contradiction for the lower ions in Equation 1 (for example, by predicting too much H I for the measured amounts of the metal ions). The higher metallicities derived from the lower ions, and our original assumption that the H I resides mainly in the lower U gas, must therefore be correct.

Nonetheless, there are still uncertainties related to the absorber's complexity; the gas does not have a single U value and we do not know how much of the H I resides co-spatially with each metal ion. We therefore estimate lower limits on the metal-to-hydrogen ratios. Hamann (1997) showed that the ionization corrections $f(\text{H I})/f(\text{M}_i)$ all have minimum values at some particular U (see also Bergeron & Stasinska 1986). If the actual absorber has zones with different U contributing to the lines, it can only mean that the true ionization corrections are larger. Therefore, the minimum ionization corrections yield

robust minimum values of [M/H]. Hamann & Ferland (1999) plot minimum ionization corrections for optically thin clouds photoionized by different power-law spectra (their Fig. 11). For the column densities in Table 2 and a spectrum similar to that adopted in §4.3, the Hamann & Ferland (1999) calculations imply lower limits of $[\text{C}/\text{H}] \gtrsim -0.7$, $[\text{N}/\text{H}] \gtrsim -0.2$, and $[\text{O}/\text{H}] \gtrsim -0.5$ for the $z_a \approx 0.9627$ absorber in 3C 288.1.

We conclude that the overall metallicity (dominated by O/H) is roughly $1/2 \text{ Z}_\odot$, with a firm lower limit near $1/3 \text{ Z}_\odot$.

4.5. Total Column Densities and Predicted X-Ray Absorption

We just argued that the H I column density is contributed mostly by a low-ionization region, where $\log U \approx -1.8$ to -1.6 and $f(\text{H I}) \approx -3.8$ to -3.5 (Fig. 4). The measured value of the H I column density (Table 2) therefore implies a total hydrogen column of $\log N_{\text{H}}(\text{cm}^{-2}) \approx 19.5$ in that region. If the metal abundances are approximately $1/2 \text{ Z}_\odot$ (§4.4), we can estimate N_{H} in the high-ionization gas from the column densities (Table 2) and ionization fractions (Fig. 4) of Ne VIII and Mg X. We find $\log N_{\text{H}}(\text{cm}^{-2}) \approx 20.2$ for that region.

These results make specific predictions for the X-ray absorption that should accompany the UV AALs. Explicit photoionization calculations, using the column densities, ionizations and abundances quoted above, imply that the continuum optical depths should be <0.016 at 0.2 keV and <0.003 at 2.0 keV (in absorber's rest frame). The deepest X-ray absorption, due mainly to the combined O VII and O VIII edges near 0.8 keV, should be $\lesssim 3\%$ below the continuum. We therefore expect no significant X-ray absorption by the AAL gas in 3C 288.1. This prediction is not sensitive to the uncertain continuum shape or any other assumptions in the calculations. The only possibility for strong X-ray absorption is if that absorber contributes negligibly to the UV lines. Such an absorber would need to have either a much lower b value or much higher ionization than we infer from the AALs.

5. Discussion

5.1. The UV–X-Ray Absorber Connection

The main results of this paper are 1) the detection of the high-ionization AALs Ne VIII $\lambda\lambda 770,780$ and Mg X $\lambda 625$, and 2) the prediction that the AAL gas will not produce significant bound-free absorption in X-rays (§4.5). Simple 1-zone models of strong UV line *and* X-ray continuum absorption cannot apply to this object. In fact, the variety of UV AALs alone requires multiple absorbing zones with different levels of ionization (§4.3). Strong X-ray absorption would require yet another zone, having a high-column density of gas with either much higher ionization or a much lower velocity dispersion (b value) than the main AAL absorber (§4.5).

To our knowledge, 3C 288.1 is now the fourth quasar for which the Ne VIII AALs (and in this case also Mg X) have been measured. The other quasars are UM 675 at redshift $z_e = 2.15$ (Hamann et al. 1995, Hamann et al. 1997), HS 1700+6416 at $z_e = 2.713$ (Petitjean et al. 1996), and J2233–606 at $z_e = 2.24$ (Petitjean & Srianand 1999). There is another object with well-measured Ne VIII, Mg X and even Si XII absorption

(SBS 1542+541 at $z_e = 2.36$, Telfer et al. 1998), but the lines in that case appear more like BALs than AALs (blueshifted by $\sim 11,500 \text{ km s}^{-1}$ and having $\text{FWHM} \approx 2500 \text{ km s}^{-1}$). It is not yet clear how common these high-ionization lines are in AAL or BAL systems, but we know of no cases where high-quality, short-wavelength spectra clearly rule out their presence. The AAL column densities measured for UM 675 and J2233–606 imply that their UV lines also form in multi-zone regions with no significant X-ray opacity. The total absorbing columns inferred from their AALs are similar to 3C 288.1, $\log N_{\text{H}}(\text{cm}^{-2}) \lesssim 20$ for solar abundances. Reliable column densities are not available for the UV absorbers in HS 1700+6416 and SBS 1542+541, although Telfer et al. (1998) estimate $\log N_{\text{H}}(\text{cm}^{-2}) \gtrsim 21.5$ for the latter BAL-like source.

Existing X-ray data are sparse for these 5 quasars with known Ne VIII absorption. The UV–X-ray spectral index of 3C 288.1, $\alpha_{ox} \approx -1.51$, implies a slightly above average X-ray/UV flux ratio for quasars of similar redshift and luminosity (Wilkes et al. 1994). While not a strong constraint on the X-ray absorption, this result is at least consistent with our prediction for negligible absorption based on the AALs alone (Brandt et al. 1999). Better data for HS 1700+6416 (Yuan et al. 1998) indicate a modest X-ray absorbing column of $\log N_{\text{H}}(\text{cm}^{-2}) \approx 20.5$. In contrast, the BAL-like source SBS 1542+541 appears to be heavily absorbed in X-rays, based on its weak X-ray flux (Telfer et al. 1998, Yuan et al. 1998).

Several recent studies describe the correlated appearance of UV and X-ray absorbers in quasars and active galaxies (§1). Brandt et al. (1999) have gone a step further by suggesting that the strengths of the UV and X-ray features also correlate. Nonetheless, the physical relationship between the absorbers remains unknown. AAL regions can clearly have a variety of properties (e.g. ionization and column density) that are not always conducive to X-ray continuum absorption (see also Kriss et al. 1996, Hamann 1997, Hamann et al. 1997, Mathur et al. 1999). Fundamentally, the column densities needed for strong AALs can be much less than those required for significant bound-free opacity. As a result, even those AAL regions with high, warm absorber-like ionizations (as in 3C 288.1, etc.) need not produce measurable X-ray absorption. Conversely, the high ionizations and high column densities derived for X-ray warm absorbers (Reynolds 1997, George et al. 1998a) will not *necessarily* produce strong AALs, especially in the lower ions if the velocity dispersion (b value) is small⁴. The two absorbing regions might be physically related in general, but they need not be identical. One specific possibility, proposed for quasar BALs (Murray et al. 1995), is that the X-ray absorption occurs at the base of an accretion-disk outflow while the UV lines form largely in the accelerated gas farther out.

Studies that encompass both the high-ionization UV lines and the high-ionization X-ray edges (e.g. O VII and O VIII) are needed to test this physical relationship further.

⁴For example, if the X-ray absorber has solar abundances and “nominal” parameters, such as $\log N_{\text{H}}(\text{cm}^{-2}) \approx 22$ and $\log U \approx 0.5$ (George et al. 1998a), then the column density in C IV will be $\log N(\text{cm}^{-2}) \lesssim 14.1$ (using ion fractions from Figure 4). The resulting line strengths depend keenly on the velocity dispersion. If the velocities are strictly thermal, then $b \approx 4.5 \text{ km s}^{-1}$ for carbon in a 15000 K gas and the equivalent width of C IV $\lambda 1548$ would be just $\sim 0.08 \text{ \AA}$ in the rest frame. At larger velocity dispersions, say $b = 20 \text{ km s}^{-1}$, this line’s strength would be $\sim 0.24 \text{ \AA}$, etc., up to $\sim 0.5 \text{ \AA}$ in the high b (optically thin) limit.

Intermediate-redshift quasars like 3C288.1 are prime targets for this work (§1). However, a special concern with quasar AALs is that they can form potentially in a variety of locations. The origin and physical nature of the AAL gas, as well as its relationship to the X-ray features, are thus intimately tied to the question of the absorber's location.

5.2. Where is the Absorber in 3C 288.1?

Recent studies indicate that AALs have generally high metallicities (near or above the solar value, e.g. Petitjean et al. 1994, Petitjean & Srianand 1999, Hamann & Ferland 1999), and strengths that correlate with the quasar's radio properties and perhaps luminosity (Anderson et al. 1987, Foltz et al. 1988, Aldcroft et al. 1994, Wills et al. 1995, Baker & Hunstead 1996, Barthel 1997, Richards et al. 1999, Brandt et al. 1999). These results suggest that AALs are often physically related to quasars. Further evidence for a close relationship has come from spectroscopic indicators, such as 1) time-variable line strengths, 2) well-resolved AAL profiles that are smooth and broad compared to thermal line widths, and 3) multiplet ratios that imply partial coverage of the background light source(s) (e.g. Barlow & Sargent 1997, Barlow et al. 1997, Hamann et al. 1997, Ganguly et al. 1999). The link between these properties and the near-quasar environment is strengthened by the fact that they are common among BALs (Barlow 1993, Barlow & Junkkarinen 1994, Hamann 1998, Arav et al. 1999). AALs with these properties are likely to form in outflows from the central engines, at radii of tens of pc or possibly much less (e.g. Hamann et al. 1997). It should be a high priority to apply these spectroscopic tests of an “intrinsic” origin to the AALs in 3C 288.1 and other sources. The existing data for 3C 288.1 provide only indirect evidence for intrinsic absorption. In particular:

- 1) The ionization (§4.3) and metallicity (§4.4) in 3C 288.1 are probably both too high for an absorber at large (cosmologically significant) distances from the QSO (Verner et al. 1994b, Hamann & Ferland 1999). The high metallicity suggests that the AAL gas resides (or originated) within the quasar's host galaxy, while the high ionization suggests a strong influence of the quasar's intense radiation field. If the gas is photoionized by the quasar spectrum, the relationship between the gas' density, ionization parameter and distance from 3C 288.1 is $R \approx 60 (1/U)^{1/2} (10^4 \text{ cm}^{-3}/n_H)^{1/2}$ pc (based on the measured flux in Fig. 1, the ionizing spectral shape used in §4.3, and a cosmology with $H_o = 65 \text{ km s}^{-1} \text{ Mpc}^{-1}$ and $q_o = 0.2$).
- 2) Three of the 5 absorption-line systems with measured Ne VIII (UM 675, J2233–606 and SBS1542+531 discussed in §5.1) are known to have at least one of the spectral indicators of an intrinsic origin listed above (Hamann et al. 1995, Hamann et al. 1997, Telfer et al. 1998, Petitjean & Srianand 1999). These results support the argument in point (1) above, that high-ionization lines like Ne VIII and Mg X are additional signatures of intrinsic absorption.
- 3) Weaker statistical evidence comes from the bipolar radio morphology of 3C 288.1 (Reid et al. 1995, Akujor et al. 1994). Lobe-dominated radio structures are known to correlate with the presence of strong AALs (Wills et al. 1995, Barthel 1997). They are also indicative of an edge-on orientation for the central quasar/accretion disk. Strong AALs (as in 3C 288.1) should therefore tend to form not only near the quasar, but near the plane of its accretion disk or extended torus (Wills et al. 1995, Barthel 1997). The

situation might be analogous to BAL outflows, where disk-like geometries are favored by polarization observations (Goodrich & Miller 1995, Hines & Wills 1995, Cohen et al. 1995) and by some theoretical models of disk-driven outflows (e.g. Murray et al. 1995, de Kool 1997).

We conclude conservatively that the AALs in 3C 288.1 are physically related to the quasar, probably forming well within the radius of the quasar's host galaxy.

5.3. The Spectral Energy Distribution

The shape of the ionizing continuum is a fundamental question in studies of quasars and active galaxies. A simple analysis of the broad emission-line equivalent widths suggests that there must be a large “blue bump,” peaking around 2–5 Rydberg and contributing more than 50% of the bolometric luminosity (e.g. Mathews & Ferland 1987, Netzer 1990). AGN spectra cannot be measured directly at these energies, but recent far-UV and soft X-ray observations give no evidence for the predicted big blue bump (Zheng et al. 1996 and Laor et al. 1997). Netzer (1985) showed that there is a serious energy budget problem in photoionization models of the emission-line gas if a strong blue bump is not included. In particular, the line strengths are severely underpredicted by the models. This theoretical problem depends partly on the global covering factor of the emitting gas. The rarity of rest-frame Lyman-limit absorption in quasars implies that we rarely (if ever) view them through the line-emitting gas; thus the covering factors are expected to be low — of order 10% (e.g. Antonnucci et al. 1989, Koratkar et al. 1992). Korista et al. (1997) recently confirmed that these low covering factors, together with the bump-less ionizing continuum inferred from the Zheng et al. and Laor et al. data, underpredict the emission line strengths by factors of several. They estimate, for example, that excessively large covering factors of 56% –75% would be needed to match the typical HeII $\lambda 1640$ line strength. One possible solution, proposed by Korista et al., is that the broad emission line regions might not “see” the same continuum shape we do.

Currently this theoretical problem is unresolved. The spectrum of 3C 288.1 presented here (§3.3) is consistent with the other observations, providing no evidence for a substantial blue bump at higher (unobserved) energies.

6. Summary and Conclusions

Comparative UV and X-ray studies are beginning to yield new insights into the nature of AGN absorbing environments. However, the the physical relationship of the UV and X-ray absorbers remains unclear. 3C 288.1 provides another counterexample to simple models that would attribute all of the UV and X-ray features to identically the same gas (see §1 for references). Realistic models must include the increasing levels of complexity implied by new and better data. Intermediate-redshift quasars will be an important source of new data because they allow us to measure a wide range of under-utilized features in the rest-frame far UV — for example the H I Lyman limit and high-ionization AALs like Ne VIII $\lambda\lambda 770,780$ and Mg X $\lambda\lambda 610,625$. Our analysis of these features in 3C 288.1 shows that multiple absorbing regions (spanning a range of ionizations, densities and/or distances from the quasar) contribute to the AAL spectrum (§4.3). Moreover, the column densities

inferred from the AALs are too small to produce significant bound-free opacity at any UV through X-ray wavelengths (§4.5). There will be no significant X-ray absorption in this object unless it occurs in yet another region — having a much higher ionization or a much lower velocity dispersion than the dominant AAL absorber. We are now pursuing X-ray observations of 3C 288.1 to test these predictions.

One essential ingredient for any model of these regions is the location of the absorbing gas. Indirect evidence suggests that the AALs in 3C 288.1 form close to the quasar, probably well within the radius of the quasar's host galaxy (§5.2). Unfortunately, that weak constraint on the location allows for a variety of possible absorption sites, e.g. interstellar gas in the extended host galaxy, a dense torus surrounding the active nucleus, or an outflow from the central engine/accretion disk. The AAL kinematics indicate that the absorber is clearly *not* part of a high-velocity wind like the BALs; the lines are only $\sim 900 \text{ km s}^{-1}$ wide and their centroids are within $\pm 1000 \text{ km s}^{-1}$ of the quasar rest frame (§4.1). Better constraints on the location and kinematics will require higher resolution spectra and, ideally, repeated observations at both UV and X-ray wavelengths (to test for variable absorption, cf. Hamann et al. 1997, Barlow & Sargent 1997, George et al. 1998b). Those data would also provide more complete and more reliable estimates of the ionizations, kinematics, abundances and column densities in the different absorbing zones.

We are grateful to Gerald Kriss and others at the Space Telescope Science Institute for their generous help with the observations and data processing. We also thank the referee, Smita Mathur, for helpful comments. Financial support for this work was provided by NASA through grant GO-07356-96A from the Space Telescope Science Institute, which is operated by the Association for Research in Astronomy, Inc., under NASA contract NAS5-26555. FH also acknowledges support from NASA through grant number NAG5-3234 in their Long Term Space Astrophysics program.

Table 1. Absorption Line Data

λ_{obs}	W_λ	ID	z_a	— $\log N(\text{cm}^{-2})$ —		Notes ^a
				$b = 200$	$b = 540$	
1180.0	0.41	
1193.5	3.10	ubl
...	1.70	O IV 608	...	15.9	15.7	ubl-i
1200.4	1.06	N I 1200	bl,mult, Gal
1206.8	1.07	S III 1206	bl, Gal
1226.3	0.27	Mg X 625	0.9622	15.0	15.0	bl
1236.0	3.78	O V 630	0.9628	16.7	15.2	FWHM=1080
1249.1	0.34	
1260.2	1.14	Si II 1260	Gal
(1265.2)	<0.25	N II 645	...	<14.2	<14.2	up
1271.1	0.19	
1290.0	0.51	S IV 657	0.9625	13.8	13.8	
1303.1	2.04	O I 1302	ubl, Gal
1330.3	0.40	S III 678	0.9628	13.5	13.5	
1335.0	1.45	C II 1335	Gal
1344.7	0.84	N III 685	0.9622	14.5	14.4	mult
(1348.5)	<0.25	C II 687	...	<14.0	<14.0	up
(1374.4)	<0.25	Ar VIII 700	...	<13.9	<13.9	up
1377.7	0.98	O III 702	0.9615	15.0	15.0	
1393.9	0.43	Si IV 1394	Gal
1399.5	0.71	
1403.0	0.95	Si IV 1403	bl?, Gal
1412.2	0.42	
1421.9	0.45	S III 724	0.9631	14.2	14.2	
1456.9	0.52	
1463.3	0.63	S IV 745	0.9645	14.5	14.4	bl
1468.5	0.85	S IV 748	0.9622	14.3	14.3	bl
(1481.7)	<0.25	Ar VI 755	...	<14.6	<14.6	up
1501.5	3.17	N IV 765	0.9624	15.4	14.8	FWHM=1140
1512.1	2.21	Ne VIII 770	0.9629	15.6	15.4	FWHM=1060
1520.7	0.31	
1527.5	1.10	Si II 1527	Gal
1532.8	1.17	Ne VIII 780	0.9643	15.5	15.4	
1536.6	0.31	
1545.7	4.31	ubl
...	0.82	S V 786	...	13.8	13.8	ubl-i

Table 1—Continued

λ_{obs}	W_λ	ID	z_a	— $\log N(\text{cm}^{-2})$ —		Notes ^a
				$b = 200$	$b = 540$	
...	2.89	O IV 788	...	15.9	15.5	ubl-i
...	0.60	C IV 1549	ubl-i, Gal
(1589.1)	<0.30	S IV 810	...	<14.4	<14.4	up
1608.1	0.56	Fe II 1608	Gal
1635.2	0.71	O III 833	0.9632	14.8	14.8	ID?
(1637.8)	<0.50	O II 834	...	<14.5	<14.5	up
1663.0	1.48	
1671.7	1.07	Al II 1671	Gal
1760.0	1.15	
1768.6	0.92	
(1774.2)	<0.50	C II 904	...	<14.1	<14.0	up
(1797.1)	<0.50	N II 916	...	<14.4	<14.3	up
1830.3	0.94	
(1831.9)	<0.50	S VI 933	...	<13.9	<13.9	
(1840.6)	<0.50	Ly ϵ 938	...	<15.7	<15.6	up
1863.5	1.49	Ly δ 950	0.9621	16.0	15.9	
1895.8	2.00	Ly γ 973	0.9493	
1909.7	2.35	Ly γ 973	0.9636	15.9	15.8	bl
1917.5	1.87	C III 977	0.9626	14.3	14.2	bl
1943.1	0.36	N III 990	0.9631	14.3	14.2	
1962.0	0.64	
1997.0	1.31	Ly β 1026	0.9469	...		
2012.8	4.13	Ly β 1026	0.9624	16.1	15.6	FWHM=1190
2025.9	5.43	O VI 1032	0.9632	16.5	15.5	FWHM=1140
2037.0	4.49	O VI 1038	0.9632	16.3	15.7	FWHM=1140
2084.2	0.67	S IV 1063	0.9613	14.9	14.9	ID?
(2127.6)	<0.40	N II 1084	...	<14.3	<14.3	up
2144.4	2.00	
2166.5	1.24	
(2194.3)	<0.40	P V 1118	...	<13.6	<13.6	up
2245.8	1.17	
2321.1	1.43	
2344.2	1.90	Fe II 2344	Gal
2366.5	4.56	Ly α 1216	0.9466	
2385.6	4.40	Ly α 1216	0.9627	15.1	14.7	
2434.7	7.21	N V 1240	0.9630	15.4	15.2	mult

Table 1—Continued

λ_{obs}	W_λ	ID	z_a	— $\log N(\text{cm}^{-2})$ —			Notes ^a
				$b = 200$	$b = 540$		
(2473.8)	<0.40	Si II 1260	...	<13.1	<13.1	up	
2586.2	0.85	Fe II 2587	Gal	
2599.8	1.24	Fe II 2600	Gal	
(2619.3)	<0.40	C II 1335	...	<14.0	<14.0	up	
(2735.5)	<0.40	Si IV 1394	...	<13.4	<13.4	up	
2796.1	1.93	Mg II 2796	Gal	
2803.9	1.39	Mg II 2804	Gal	
2854.2	0.50	Mg I 2853	Gal	
3040.1	7.13	C IV 1549	0.9625	15.0	14.8	mult	

^aAbbreviations have the following meanings: bl = blended line measured separately, ubl = unresolved blend, ubl-i = unresolved blend with individual W_λ estimated, FWHM = full width at half minimum in km s^{-1} , Gal = Galactic line, ID? = identification uncertain, mult = unresolved multiplet listed as one line, up = 3σ upper limits at λ_{obs} defined by $z_a = 0.9627$.

Table 2. Column Densities

Ion	$\log N(\text{cm}^{-2})$ $b = 300$
H I	15.8
C II	<14.0
C III	14.3:
C IV	14.9
N II	<14.2
N III	14.4
N IV	15.0
N V	15.2
O II	<14.5
O III	14.9
O IV	15.7
O V	15.6:
O VI	15.8
Ne VIII	15.4
Mg X	15.0:
Si II	<13.1
Si IV	<13.4
P V	<13.6
S II	<13.5
S III	14.0::
S IV	14.2::
S V	13.8::
S VI	<13.9

REFERENCES

Akujor, C.E., Lüdke, E., Browne, I.W.A., Leahy, J.P., Garrington, S.T., Jackson, N., & Thomasson, P. 1994, *A&AS*, 105, 247

Aldcroft, T.L., Bechtold, J., & Elvis, M. 1994, *ApJS*, 93, 1

Anderson, S.f., Weymann, R.J., Foltz, C.B., & Chaffee, F.H. 1987, *AJ*, 94, 278

Antonucci, R.R.J., Kinney, A.L., & Ford, H.C. 1989, *ApJ*, 342, 64

Arav, N., Korista, K.T., de Kool, M., Junkkarinen, V.T., & Begelman, M.C. 1999, *ApJ*, 516, 27

Baker, J.C., & Hunstead, R.W. 1996, *ApJ*, 452, L95

Barlow, T.A. 1993, *Ph.D. Dissertation*, University of California, San Diego

Barlow, T.A., Hamann, F., & Sargent, W.L.W. 1997, in Mass Ejection From AGN, eds. R. Weymann, I. Shlosman, and N. Arav, *ASP Conf. Series*, 128, 13

Barlow, T.A., & Sargent, W.L.W. 1997, *AJ*, 113, 136

Barthel, P. 1997, in Mass Ejection From AGN, eds. R. Weymann, I. Shlosman, and N. Arav, *ASP Conf. Series*, 128, xxx

Bergeron, J., & Stasinska, G. 1986, *A&A*, 169, 1

Brandt, W.N., Laor, A., & Wills, B.J. 1999, *ApJ*, in press

Cohen, M.H., Ogle, P.M., Tran, H.D., Vermeulen, R.C., Miller, J.S., Goodrich, R.W., & Martel, A.R. 1995, *ApJ*, 448, L77

Crenshaw, D.M., Kraemer, S.B., Boggess, A., Maran, S.P., Mushoktzky, R.F., & Wu, C.-C. 1999, *ApJ*, 516, 750

de Kool, M. 1997, in Mass Ejection From AGN, eds. R. Weymann, I. Shlosman, and N. Arav, *ASP Conf. Series*, 128, 233

Ferland, G.J., Korista, K.T., Verner, D.A., Ferguson, J.W., & Kingdon, J.B. 1998, *PASP*, 110, 761

Foltz, C.B., Chaffee, F., Weymann, R.J., & Anderson, S.F. 1988, in QSO Absorption Lines: Probing the Universe, eds. JC Blades, DA Turnshek, CA Norman (Cambridge: Cambridge Univ Press), p. 53

Foltz, C.B., Weymann, R.J., Peterson, B.M., Sun, L., & Malkan, M.A., et al. 1986, *ApJ*, 307, 504

Gallagher, S.C., Brandt, W.N., Sambruna, R.M., Mathur, S., & Yamasaki, N. 1999, *ApJ*, in press

Ganguly, R., Eracleous, M., Charlton, J.C., & Churchill, C.W. 1999, *AJ*, 117, 2594

George, I.M., Turner, T.J., Mushotzky, R.F., H., Nandra, & Netzer, H. 1998b, *ApJ*, 503, 174

George, I.M., Turner, T.J., Netzer, H., Nandra, K., Mushotzky, R.F., & Yaqoob, T. 1998a, *ApJS*, 114, 73

Goodrich, R. W., & Miller, J. S. 1995, *ApJ*, 448, L73

Green, P.J., & Mathur, S. 1996, *ApJ*, 462, 637

Grevesse, N., & Anders, E. 1989, in *Cosmic Abundances of Matter*, AIP Conf. Proc. 183, ed. C.I. Waddington (New York:AIP), 1

Hamann, F. 1997, *ApJS*, 109, 279

Hamann, F. 1998, *ApJ*, 500, 798

Hamann, F., Barlow, T.A., Beaver, E.A., Burbidge, E.M., Cohen, R.D., Junkkarinen, V., & Lyons, R. 1995, *ApJ*, 443, 606

Hamann, F., Barlow, T.A., Junkkarinen, V.T., & Burbidge, E.M. 1997, *ApJ*, 478, 80

Hamann, F., Barlow, T.A., Weymann, R.J., Chaffee, F., & Foltz, C. 1999, in preparation.

Hamann, F., Cohen, R.D., Shields, J.C., Burbidge, E.M., Junkkarinen, V.T., & Crenshaw, D.M. 1998, *ApJ*, 496, 761

Hamann, F., & Ferland, G.J. 1999, *ARA&A*, 37, in press

Hines, D.C., & Wills, B.J. 1995, *ApJ*, 448, L69

Barlow, T.A., & Junkkarinen, V.T. 1994, *BAAS*, 26, 1339

kora92] Koratkar, A.P., Kinney, A.L., & Bohlin, R.C. 1992, *ApJ*, 400, 435

Korista, K. T., Ferland, G., & Baldwin, J. 1997, *ApJ*, 487, 555

Kriss, G.A., Espey, B.R., Krolik, J.H., Tsvetanov, Z., Zheng, W., & Davidsen, A.F. 1996, *ApJ*, 467, 622

Laor, A., Fiore, F., Elvis, M., Wilkes, B. J., & McDowell, J. C. 1997, *ApJ*, 477, 93

Marziani, P., Sulentic, J.W., Dultzin-Hacyan, D., Calvani, M., & Moles, M. 1996, *ApJS*, 104, 37

Mathur, S., Elvis, M., & Wilkes, B. 1999, *ApJ*, 519, 605

Mathur, S., Wilkes, B., & Elvis, M. 1998, *ApJ*, 503, L23

Morris, S.L., Weymann, R.J., Foltz, C.B., Turnshek, D.A., Shectman, S., Price, C., & Boroson, T.A. 1986, *ApJ*, 310, 40

Murray, N., Chiang, J., Grossman, S.A., & Voit, G.M. 1995, *ApJ*, 451, 498

Netzer, H. 1985, *ApJ*, 289, 451

Netzer, H. 1990, in *Active Galactic Nuclei*, eds. R.D. Blandford, H. Netzer, L. Woltjer, (Berlin:Springer), 57

Netzer, H. 1996, *ApJ*, 473, 781

O'Brien, P.T., Gondhalekar, P.M., & Wilson, R. 1988, *MNRAS*, 233, 801

Petitjean, P., Rauch, M., & Carswell, R. F. 1994, *A&A*, 291, 29

Petitjean, P., Riediger, R., & Rauch, M. 1996, *A&A*, 307, 417

Petitjean, P., & Srianand, R. 1999, *A&A*, 345, 73

Reid, A., Shone, D.L., Akujor, C.E., Browne, I.W.A., Murphy, D.W., & Walsh, D. 1997, *A&AS*, 110, 213

Reynolds, C. S. 1997, *MNRAS*, 286, 513

Richards, G.T., York, D.G., Yanny, B., Kollgaard, R.I., Laurent-Muehleisen, S.A., et al. 1999, *ApJ*, 513, 576

Sargent, W.L.W., Boksenberg, A. & Young, P. 1982, *ApJ*, 252, 54

Shields, J.C., & Hamann, F. 1997, *ApJ*, 481, 752

Schmidt, M. 1968, *ApJ*, 151, 393

Schneider, D.P., et al. 1993, *ApJS*, 87 45

Telfer, R. C., Kriss, G. A., Zheng, W., Davidson, A. F., & Green, R. F. 1998, *ApJ*, 509, 132

Tripp, T.M., Lu, L., & Savage, B.D. 1996, *ApJS*, 102, 239

Turnshek, D. A. 1995, in *QSO Absorption Lines*, ed. G. Meylan, (Berlin:Springer-Verlag), 223

Verner, D.A., Barthel, P.D., & Tytler, D., 1994a, *A&AS*, 108, 287

Verner, D.A., Tytler, D., & Barthel, P.D. 1994b, *ApJ*, 430, 186

Wampler, E. J., Bergeron, J., & Petitjean, P. 1993, *A&A*, 273, 15

Weymann, R.J. 1997, in *Mass Ejection From AGN*, eds. R. Weymann, I. Shlosman, and N. Arav, *ASP Conf. Series*, 128, 3

Weymann, R. J. 1995, in *QSO Absorption Lines*, ed. G. Meylan, (Berlin:Springer-Verlag), 213

Weymann, R. J., Turnshek, D. A., & Christiansen, W. A. 1985, in *Astrophysics of Active Galaxies and Quasi-Stellar Objects*, ed. J. Miler, (Mill Valley:Univ. Sci. Books), 185

Weymann, R.J. Williams, R.E., Peterson, B.M., & Turnshek, D.A. 1979, *ApJ*, 218, 619

Wilkes, B.J., Tananbaum, H., Worrall, D.M., Avni, Y., Oey, M.S., & Flanagan, J. 1994, *ApJS*, 92, 53

Williams, R.E., Strittmatter, P.A., Carswell, R.F., & Craine, E.R. 1975, *ApJ*, 202, 296

Wills, B.J., Thompson, K.L., Han, M., Netzer, H., Wills, D. et al. 1995, *ApJ*, 447, 139

Yuan, W., Brinkmann, W., Siebert, J., & Voges, W. 1998, *A&A*, 330, 108

Zamorani, G., et al. 1981, *ApJ*, 245, 357

Zheng, W., Kriss, G.A., Telfer, R.C., Grimes, J.P., & Davidson, A.F. 1997, *ApJ*, 475, 469

FIGURE CAPTIONS

Fig. 1. — *HST* STIS spectra of 3C 288.1 at both the observed and rest-frame wavelengths (where rest is defined by the emission redshift $z_e = 0.961$). The upper and lower panels show spectra from the G140L and G230L gratings, respectively. The Flux has units 10^{-15} ergs s^{-1} cm^{-2} \AA^{-1} . Absorption lines in the main AAL system ($z_a \approx 0.9627$) are labeled across the top. Galactic lines and a weaker Ly α system (at $z_a \approx 0.9467$) are marked below.

Fig. 2. — Observed spectrum of 3C 288.1 (solid histogram) and a fit (dotted lines) to the continuum, O VI emission line, and several absorption lines. The Ly β line at the left has redshift $z_a \approx 0.9467$, while the others belong to the strong associated system at $z_a \approx 0.9627$ (see Fig. 1 and §3.1).

Fig. 3. — Spectrum of 3C 288.1 on a log-log scale, where ν is the rest-frame frequency in Hz and the flux F_ν has units ergs s^{-1} cm^{-2} Hz^{-1} . The bold solid line is a broken power law with $\alpha = -1.73$ for $\log \nu(\text{Hz}) \gtrsim 15.46$ and $\alpha \approx -0.83$ for $\log \nu(\text{Hz}) \lesssim 15.46$. The dotted line is just an extension of the low frequency power law segment. “LL” marks the Lyman limit in the $z_a \approx 0.9627$ absorption system.

Fig. 4. — Ionization fractions in optically thin clouds that are photoionized at different U . The ionizing spectrum is a broken power-law with $\alpha_{uvx} = -1.7$ and $\alpha_x = -0.9$. The HI fraction appears across the top. The curves for the metal ions are labeled directly above or below their maximum values, except for Mg II in the lower left of the bottom panel. The sulfur ions in the lower panel, and silicon ions in the upper panel, are represented by dash-dot curves for clarity. The notation is HI = H 0 , CIV = C $^{+3}$, etc. The bold vertical lines connect pairs of $f(M_i)$ curves at the U value implied by the ratio of their column densities. Specifically, the bold lines correspond to the ratios C III/C IV, O IV/O V, O III/O IV, O V/O VI, O VI/Ne VIII, and Ne VIII/Mg X from left to right in the top panel, and S IV/S V, S III/S IV, N III/N IV, and N IV/N V in the bottom panel. See §4.3.

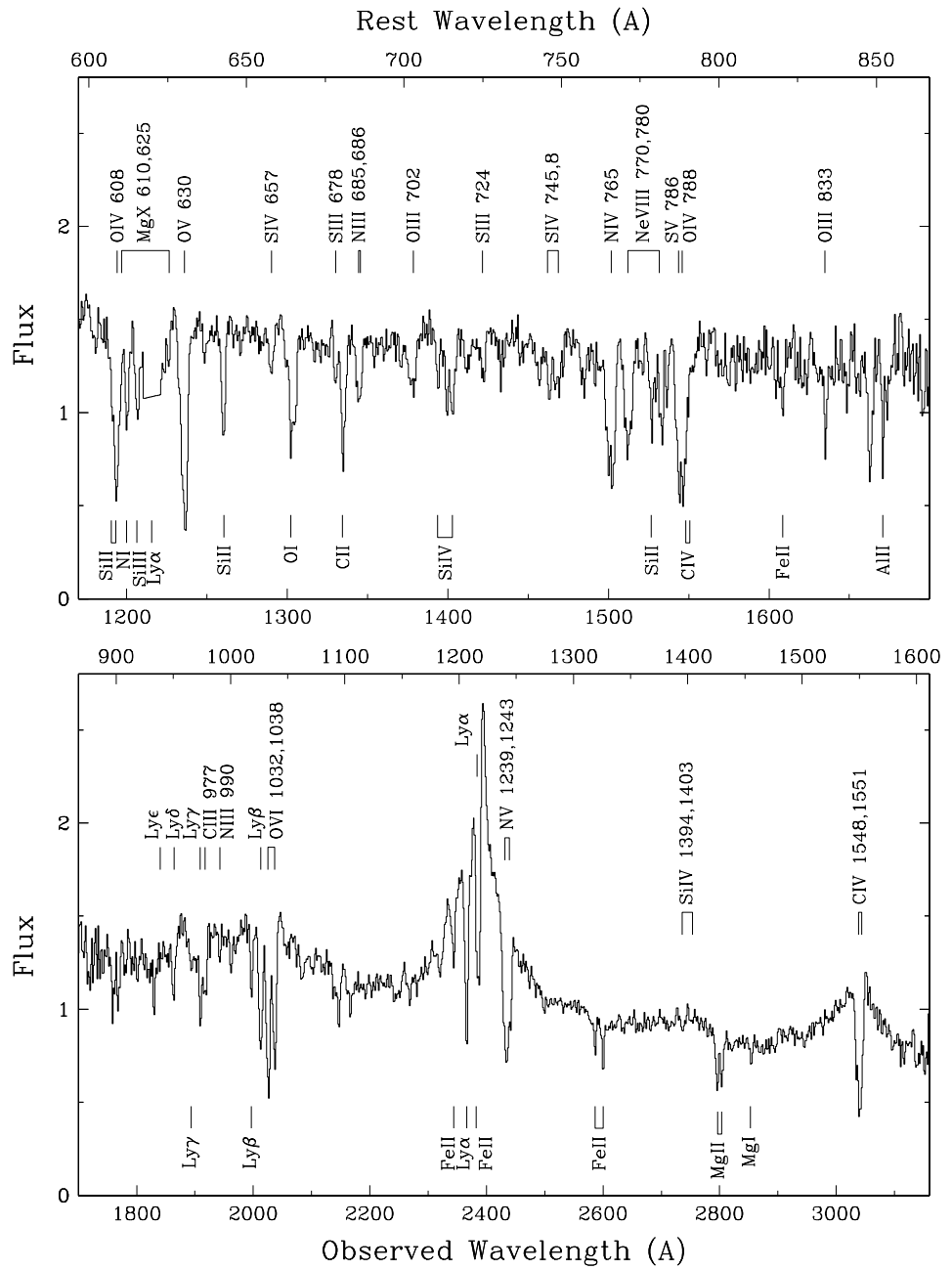


FIGURE 1.

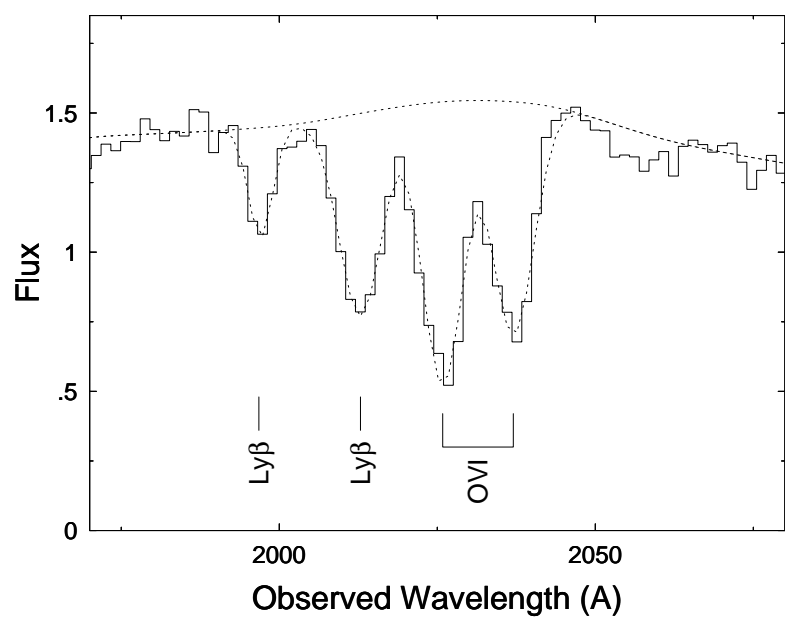


FIGURE 2.

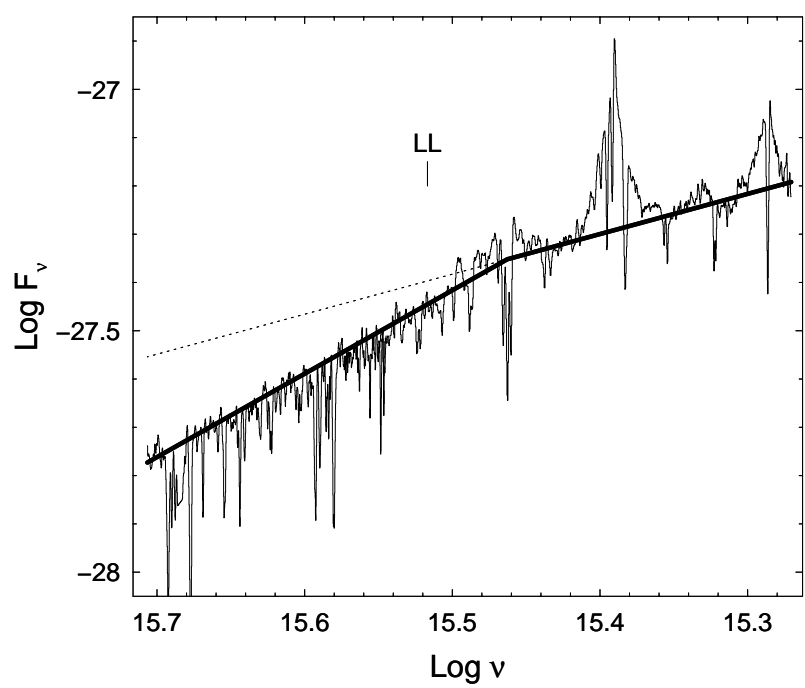


FIGURE 3.

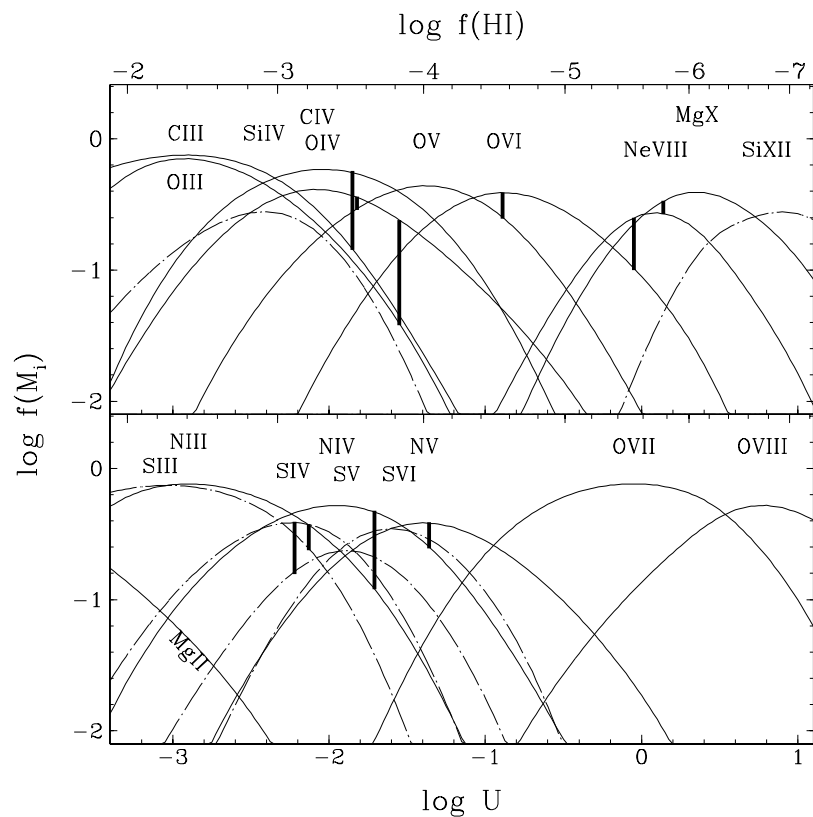


FIGURE 4.